

Surprising absence of strong homonuclear coupling at low magnetic field explored by two-field NMR spectroscopy

Ivan V. Zhukov,^{1,2} Alexey S. Kiryutin,^{1,2} Ziqing Wang,³ Milan Zachrdla,³ Alexandra V. Yurkovskaya,^{1,2} Konstantin L. Ivanov,^{1,2,*} Fabien Ferrage^{3*}

¹ International Tomography Center, Siberian Branch of the Russian Academy of Sciences, Novosibirsk, 630090, Russia

² Novosibirsk State University, Novosibirsk, 630090, Russia

³ Laboratoire des Biomolécules, LBM, Département de chimie, École normale supérieure, PSL University, Sorbonne Université, CNRS, 75005 Paris, France

* Konstantin L. Ivanov, ivanov@tomo.nsc.ru

* Fabien Ferrage, fabien.ferrage@ens.psl.eu

Abstract

Strong coupling of nuclear spins, which is achieved when their scalar coupling $2\pi J$ is greater than or comparable to the difference $\Delta\omega$ in their Larmor precession frequencies in an external magnetic field, gives rise to efficient coherent longitudinal polarization transfer. The strong-coupling regime can be achieved when the external magnetic field is sufficiently low, as $\Delta\omega$ is reduced proportional to the field strength. In the present work, however, we demonstrate that in heteronuclear spin systems these simple arguments may not hold, since heteronuclear spin-spin interactions alter the $\Delta\omega$ value. The experimental method that we use is two-field NMR (Nuclear Magnetic Resonance), exploiting sample shuttling between a high field, at which NMR spectra are acquired, and low field, where strong couplings are expected, at which NMR pulses can be applied to affect the spin dynamics. By using this technique, we generate zero-quantum spin coherences by means of non-adiabatic passage through a level anti-crossing and study their evolution at low field. Such zero-quantum coherences mediate the polarization transfer under strong coupling conditions. Experiments performed with an ^{13}C labelled amino acid clearly show that the coherent polarization transfer at low field is pronounced in the ^{13}C -spin subsystem under proton decoupling. However, in the absence of proton decoupling, polarization transfer by coherent processes is dramatically reduced, demonstrating that heteronuclear spin-spin interactions suppress the strong coupling regime even when the external field is low. A theoretical model is presented, which can simulate the reported experimental results.

35 I. Introduction

36 The topological and conformational information provided by scalar couplings lies at the foundation of the
37 analytical power of NMR spectroscopy (Ernst et al., 1987; Keeler, 2005; Levitt, 2008; Cavanagh, 2007). The
38 strong coupling case is encountered when scalar coupling constants are not negligible with respect to the
39 difference of resonance frequency between the coupled spins (Keeler, 2005). Understanding strong scalar
40 couplings and their spectral signature was essential when NMR was introduced for chemical analysis,
41 which was typically performed at magnetic fields considered today as low (Bodenhausen et al., 1977;
42 Pfändler and Bodenhausen, 1987). Modern high-field NMR is widely based on the exploitation of weak
43 scalar couplings, so that strong scalar couplings have remained a nuisance, in particular in aromatic spin
44 systems (Vallurupalli et al., 2007; Foroozandeh et al., 2014). Recently, the development and availability of
45 benchtop NMR spectrometers operating at low or moderate magnetic fields (Grootveld et al., 2019), has
46 revived the interest in the understanding of strong scalar couplings in conventional NMR.

47 Contrarily to conventional NMR, NMR at near-zero or ultralow magnetic fields (ZULF-NMR), explores the
48 benefits of NMR in the strong scalar-coupling regime. At such magnetic fields, typically smaller than 1 μT ,
49 scalar coupling interactions dominate all Zeeman interaction and dictate the eigenstates of spin systems
50 and transition energies obtained in spectra (Ledbetter et al., 2011; Tayler et al., 2017; Blanchard and
51 Budker, 2016). However, for homonuclear couplings, the transition between the weak- and strong-
52 coupling regimes occurs in a range of magnetic fields, where the Zeeman interaction is still dominant
53 (Ivanov et al., 2006; Ivanov et al., 2008; Ivanov et al., 2014; Appelt et al., 2010; Türschmann et al., 2014).
54 This transition between weak and strong couplings can be investigated by varying the magnetic field
55 applied to the sample on a high-field magnet, which is usually performed by moving the sample through
56 the stray field with a shuttle system (Roberts and Redfield, 2004a, b; Redfield, 2012; Wagner et al., 1999;
57 Bryant and Korb, 2005; Goddard et al., 2007; Chou et al., 2016; Chou et al., 2017; Charlier et al., 2013;
58 Cousin et al., 2016a; Cousin et al., 2016b; Zhukov et al., 2018; Kiryutin et al., 2016). These studies have
59 highlighted the effects of level anti-crossings (LACs) (Miesel et al., 2006; Ivanov et al., 2014). When the
60 passage through a LAC is slow, the transition is adiabatic and the population of eigenstates is smoothly
61 converted to the new eigenstates. When the transition is fast, coherences can be generated between the
62 new eigenstates and time-oscillations of the population of high-field eigenstates can be observed
63 (Pravdivtsev et al., 2013; Kiryutin et al., 2013). This phenomenon has been observed on a variety of
64 homonuclear spin systems. Heteronuclear scalar couplings have been shown to alter LACs in homonuclear
65 spin systems (Korchak et al., 2012); yet, the properties of such heteronuclear couplings on LACs are not
66 fully understood, in particular, in spin systems with extensive networks of homo- and heteronuclear scalar
67 couplings. As usual, non-adiabatic variation, which gives rise to excitation of coherences, means that the
68 adiabatic eigenstates of the spin system change with time fast as compared to the rate of internal
69 evolution of the system. Specifically, for each pair of adiabatic states, $|i\rangle$ and $|j\rangle$, the parameter

$$70 \quad \xi_{ij} = \frac{\langle j | \frac{d}{dt} | i \rangle}{\omega_{ij}}$$

71 Is much greater than 1 (here ω_{ij} is the energy difference between the states, measured in angular
72 frequency units). When $\xi_{ij} \ll 1$, switching is adiabatic and populations follows the time-dependent
73 eigenstates.

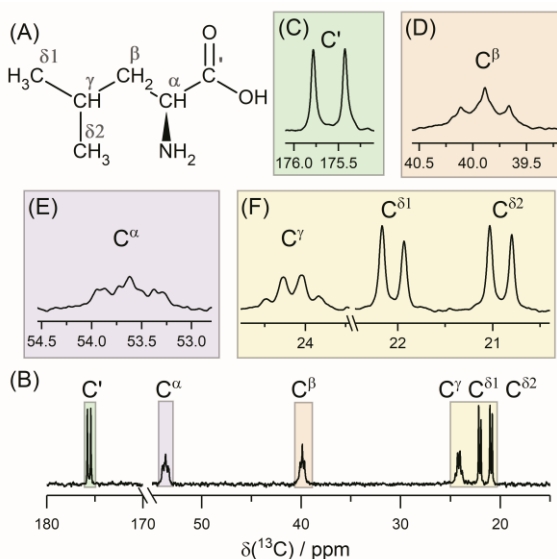
74 Here, we investigate the effect of heteronuclear scalar couplings on LACs in a spin system typical of
75 biomolecular NMR, a uniformly carbon-13 labeled amino acid (leucine), which combines extensive
76 networks of homo- and heteronuclear scalar couplings. Essentially, we exploit the ability to apply
77 composite pulse decoupling on our two-field NMR spectrometer (Cousin et al., 2016a) to switch on and
78 off heteronuclear scalar couplings at low magnetic field. We demonstrate that heteronuclear scalar
79 couplings alter LACs by sustaining the weak-coupling regime in a carbon-13 homonuclear spin system.

80 Composite pulse decoupling at low magnetic field restores the strong scalar coupling regime in the
 81 carbon-13 nuclei of the isopropyl group of leucine at 0.33 T. Our results identify how heteronuclear
 82 couplings alter homonuclear couplings at low magnetic fields, which could be exploited in low-field NMR
 83 methodology and may be considered in further developments of total correlation spectroscopy (TOCSY)
 84 (Braunschweiler and Ernst, 1983) mixing sequences in high-field NMR.

85 II. Methods

86 A. Sample preparation

87 Experiments have been performed using the following sample: 76 mM 99% enriched $^{13}\text{C},^{15}\text{N}$ labeled L-
 88 leucine (Leu) in 90% H_2O 10% D_2O solution. $^{13}\text{C},^{15}\text{N}$ enriched L-leucine were purchased from Sigma-Aldrich
 89 and used as it stands. ^{13}C -NMR spectrum of the labelled Leu molecule is shown in **Figure 1**. We also show
 90 separately the signals of the individual carbon nuclei. Broadband proton decoupling was used to simplify
 91 the spectrum. Here, we will focus on a three-spin system, formed by the C^γ and two C^δ nuclei of the
 92 isopropyl moiety. We will study polarization transfer in this subsystem upon fast switch of the external
 93 magnetic field obtained by a transfer of the sample though the stray field of a high-field NMR magnet.



94

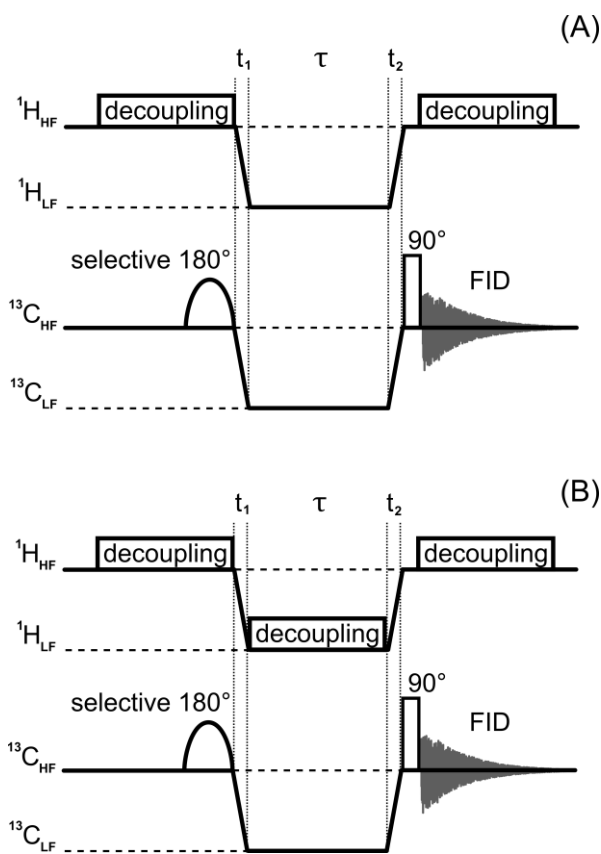
95 **Figure 1.** Structure of $^{13}\text{C},^{15}\text{N}$ L-leucine (A) and 150.9 MHz ^{13}C -NMR spectrum (B) under broadband ^1H decoupling.
 96 Signal of each carbon nuclei is also shown separately (C)-(E). The multiplet structure in the spectrum is due to ^{13}C -
 97 ^{13}C and ^{13}C - ^{15}N scalar interactions.

98 B. Field-cycling NMR experiments

99 NMR experiments were performed on a two-field NMR spectrometer (Cousin et al., 2016a) with fast
 100 sample shuttling (Charlier et al., 2013). The high field $B_{HF} = 14.1$ T is the detection field of a 600 MHz
 101 NMR spectrometer while the low field is $B_{LF} = 0.33$ T corresponding to 14 MHz ^1H NMR frequency. The
 102 magnetic field in the low-field centre is sufficiently homogeneous (inhomogeneities of the order of 10
 103 ppm) so that radiofrequency (RF) pulses can be applied by using a triple-resonance NMR probe, as
 104 described previously (Cousin et al., 2016a).

105 Field-cycling NMR experiments were run according to the pulse sequences depicted in **Figure 2**. First, a
 106 non-equilibrium state is generated at B_{HF} by applying a selective π pulse to the $\text{C}^{\delta 2}$ nucleus (shaped RE-
 107 BURP pulse (Geen and Freeman, 1991), the pulse duration was 46.4 ms, the peak RF-field amplitude was
 108 adjusted to cover *ca.* 100 Hz bandwidth around the center of $\text{C}^{\delta 2}$ signal). RE-BURP shaped pulse was used
 109 since it is less sensitive to the initial nuclear magnetization state than I-BURP (Geen and Freeman, 1991)
 110 and has narrow excitation profile. To improve the selectivity of the pulse, simultaneous proton decoupling
 111 was used, which reduces multiplet overlap in the carbon-13 NMR spectrum. Following this preparation,

112 the sample was shuttled from the high-field center to the low-field center $B_{HF} \rightarrow B_{LF}$ with a duration
 113 $t_1 = 110$ ms. The field jump is fast enough to be non-adiabatic and it is aimed to excite a spin coherence.
 114 Subsequently, the coherence evolves at B_{LF} during a variable time period τ . The shuttle transfer back to
 115 the high-field center leads to a second field jump $B_{LF} \rightarrow B_{HF}$ with a duration $t_2 = 95$ ms. This second non-
 116 adiabatic field jump to B_{HF} converts the coherence into a population difference. Detection is performed
 117 after a $\pi/2$ pulse on the carbon-13 channel in the presence of proton decoupling. We perform two types
 118 of experiments, in which the carbon spin coherence (zero-quantum coherence, ZQC) evolves at B_{LF} in the
 119 absence (see **Figure 2A**) and in the presence (see **Figure 2B**) of proton composite-pulse decoupling.
 120 Decoupling at B_{LF} has been performed using composite pulse decoupling pulse with the WALTZ
 121 decoupling with MLEV-64 supercycle (Shaka et al., 1983; Levitt et al., 1982) at low field on the proton RF-
 122 channel (operating at 14 MHz corresponding to the proton NMR frequency at 0.33 T). Composite pulse
 123 decoupling is used because of the rather high inhomogeneity of the B_{LF} field, which is of the order of 10
 124 ppm: under such conditions continuous-wave decoupling would require higher power, potentially giving
 125 rise to sample heating. The τ -dependence of polarization is expected to be oscillatory, due to the coherent
 126 polarization exchange within the expectedly strongly coupled system of the C^γ and two C^δ carbon-13
 127 nuclei.



128 **Figure 2.** Experimental protocols of field-cycling NMR experiments without ^1H decoupling at the low field (A) and
 129 with 24 kHz WALTZ-64 ^1H decoupling at the low field (B). Details of the experiments: 0.56 W (10 KHz) WALTZ-64
 130 composite pulse decoupling on the proton channel was applied at B_{HF} during 100 ms prior to a selective 180 -degree
 131 pulse, in order to enhance ^{13}C polarization by the nuclear Overhauser effect. The sample shuttle times, t_1 and t_2 ,
 132 were 80 ms and 120 ms, respectively. Selective inversion was performed with a ReBurrp pulse (Geen and Freeman,
 133 1991) with a duration of 46.4 ms at the $C^{\delta 2}$ resonant frequency covering *ca.* 100 Hz bandwidth. The delay τ at low
 134 field was incremented with a 5 ms step. After sample transfer to high field, a hard 90 -degree pulse generated ^{13}C
 135 transverse magnetization; FID acquisition was done during 1.56 s under 2.7 kHz WALTZ-64 proton decoupling.
 136

137 III. Theory

138 A. Polarization transfer in a 3-spin system

139 In this subsection, we provide a theoretical description of the field-cycling NMR experiments. First, we
 140 present the analytical treatment of polarization transfer among two nuclei of the same kind, here spin I_1
 141 and spin I_2 (e.g. two carbon-13 nuclei), in the presence of a third spin S , which can be a heteronucleus
 142 (e.g. here a proton). This is the minimal system allowing us to detail the effect of a heteronucleus on
 143 polarization transfer among strongly coupled spins. We assume that spins I_1 and I_2 are in strong coupling
 144 conditions, meaning that the difference, $\Delta\omega$, in their Zeeman interaction frequencies with the external
 145 field is smaller than or comparable to the scalar-coupling constant, $2\pi J_{12}$, between them. When the
 146 strong coupling regime is achieved, the zero-quantum part of the scalar coupling, given by the operator
 147 $\{\hat{I}_{1+}\hat{I}_{2-} + \hat{I}_{1-}\hat{I}_{2+}\}$, becomes active, giving rise to flips and flops of spins I_1 and I_2 . The couplings to the
 148 third spin S , J_{13} and J_{23} , are assumed to be unequal (otherwise coupling to the proton gives rise to an
 149 identical shift of the NMR frequencies of spins 1 and 2 and does not modify the eigenstates of this
 150 subsystem). The Hamiltonian of the spin system can be written as follows (in \hbar units):

$$\hat{\mathcal{H}}_{CCH} = -\omega_1\hat{I}_{1z} - \omega_2\hat{I}_{2z} - \omega_3\hat{S}_z + 2\pi J_{12}(\hat{\mathbf{I}}_1 \cdot \hat{\mathbf{I}}_2) + 2\pi J_{13}\hat{I}_{1z}\hat{S}_z + 2\pi J_{23}\hat{I}_{2z}\hat{S}_z \quad (1)$$

151 Here $\hat{\mathbf{I}}_1$, $\hat{\mathbf{I}}_2$ and $\hat{\mathbf{S}}$ are the spin operators; $\omega_1 = \gamma_I(1 + \delta_1)B$, $\omega_2 = \gamma_I(1 + \delta_2)B$ and $\omega_3 = \gamma_S(1 + \delta_3)B$
 152 stand for the NMR frequencies of the corresponding nuclei (with $\gamma_{I,S}$ being the corresponding
 153 gyromagnetic ratios, δ_i being the chemical shifts and B being the magnetic field strength). We assume
 154 that the heteronucleus S is coupled weakly to I spins due to the large difference in their NMR frequencies,
 155 i.e., $|\omega_1 - \omega_3|, |\omega_2 - \omega_3| \gg |\omega_1 - \omega_2|, 2\pi J_{13}, 2\pi J_{23}$, and keep only the secular part of the heteronuclear
 156 coupling Hamiltonian.

157 In the present case, the nuclear magnetic number, m_S , of spin S is a “good quantum number”, which is
 158 conserved because \hat{S}_z commutes with the Hamiltonian. For this reason, it is possible to find the solution
 159 for the spin dynamics of spins I_1 and I_2 for two separate cases, which corresponds to the two different
 160 values of m_S being $+\frac{1}{2}$ and $-\frac{1}{2}$, i.e., spin S is in the “spin-up” $|\alpha\rangle$ state or “spin-down” $|\beta\rangle$ state. In each
 161 case, the Hamiltonian of the carbon subsystem is as follows:

$$\hat{\mathcal{H}}_{CC} = -\{\omega_1 - 2\pi J_{13}S_z\}\hat{I}_{1z} - \{\omega_2 - 2\pi J_{23}S_z\}\hat{I}_{2z} + 2\pi J_{12}(\hat{\mathbf{I}}_1 \cdot \hat{\mathbf{I}}_2) \quad (2)$$

162 Hence, in the Hamiltonian given by eq. (1) we replace the \hat{S}_z operator by the m_S value, which is $\pm\frac{1}{2}$. Hence,
 163 the $\Delta\omega$ value is modified and it depends on the m_S value:

$$\Delta\omega_{\pm} = \{\omega_1 - \omega_2\} \mp \pi\{J_{13} - J_{23}\} = \Delta\omega \mp \pi \cdot \Delta J \quad (3)$$

164 The eigenstates of the subsystem of spin 1 and spin 2 are

$$\begin{aligned} |1\rangle &= |\alpha\alpha\rangle, \quad |2\rangle_{\pm} = \cos\theta_{\pm}|\alpha\beta\rangle + \sin\theta_{\pm}|\beta\alpha\rangle \\ |3\rangle_{\pm} &= -\sin\theta_{\pm}|\alpha\beta\rangle + \cos\theta_{\pm}|\beta\alpha\rangle, \quad |4\rangle = |\beta\beta\rangle \end{aligned} \quad (4)$$

165 Here the “mixing angle” is given by the values of $\Delta\omega_{\pm}$ and J_{12} : $\tan 2\theta_{\pm} = 2\pi J_{12}/\Delta\omega_{\pm}$. When $\Delta\omega_{\pm}$
 166 approaches zero, the mixing angle goes to $\frac{\pi}{4}$ meaning that the eigenstates become singlet and triplet
 167 states: the spins are strongly coupled. When $\Delta\omega_{\pm}$ is much greater than the coupling, the eigenstates are
 168 obviously the Zeeman states.

169 Even in this simple system, it is clear that the condition $|\omega_1 - \omega_2| \ll 2\pi J_{12}$ is not sufficient to guarantee
 170 strong coupling of the two carbons. Indeed, when $2\pi\Delta J$ is greater than $\Delta\omega$ and $2\pi J_{12}$ the carbon spins
 171 become weakly coupled in the two sub-ensembles, corresponding to $m_S = \pm\frac{1}{2}$.

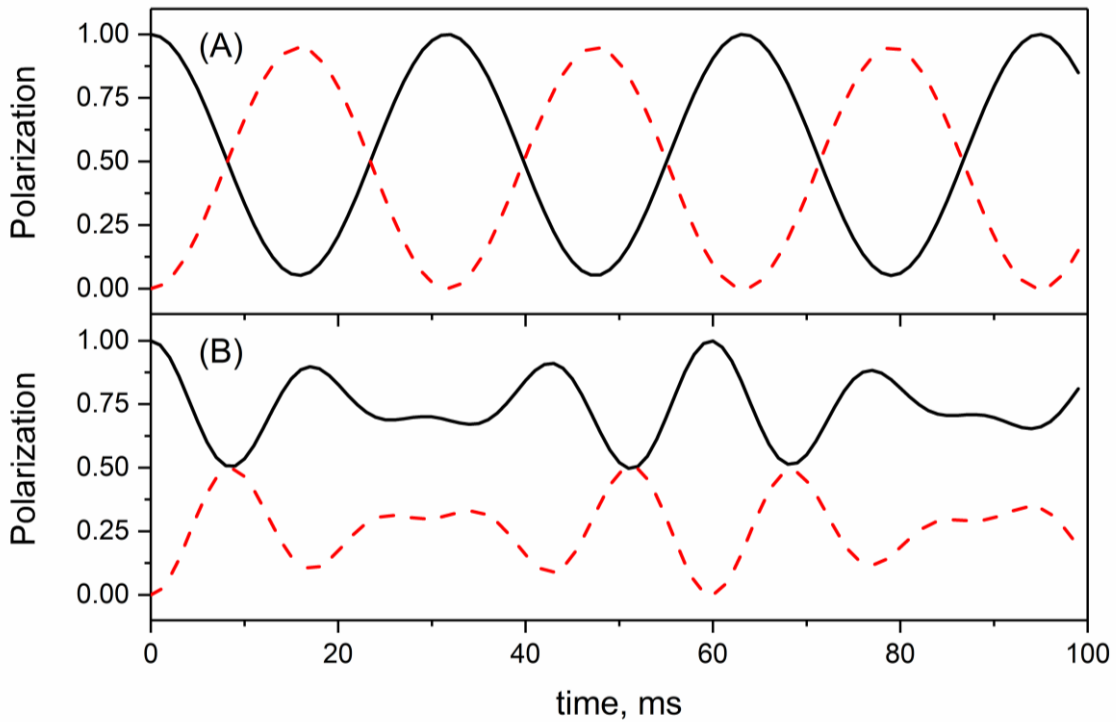
172 How do heteronuclear couplings affect polarization transfer in the carbon system? We assume that at $t =$
 173 0 one of the spins has polarization $\langle I_{1z} \rangle = P_0$ and the other spin is not polarized, $\langle I_{2z} \rangle = 0$. Hereafter, it
 174 is convenient to use normalization $P_0 = 1$. The state of the spin system is then given by the density
 175 operator

$$\sigma_0 = \hat{I}_{1z} \quad (5)$$

176 As shown previously (Ivanov et al., 2006), in the two-spin system of I_1 and I_2 , in the absence of coupling
177 to any other spin, the polarization evolves with time as follows:

$$\langle I_{1z} \rangle(t) = 1 - \sin^2 \theta \frac{1 - \cos[\omega_{ZQC} t]}{2}, \quad \langle I_{2z} \rangle(t) = \sin^2 \theta \frac{1 - \cos[\omega_{ZQC} t]}{2} \quad (6)$$

178 where $\tan 2\theta = 2\pi J_{12}/\Delta\omega$ and the oscillation frequency $\omega_{ZQC} = \sqrt{\Delta\omega^2 + (2\pi J_{12})^2}$ is the frequency of
179 the ZQC between the eigenstates $|2\rangle$ and $|3\rangle$. Hence, coherent exchange of polarization is taking place.
180 As $\Delta\omega$ becomes smaller the frequency of the oscillations decreases, but the amplitude increases: at $\Delta\omega \rightarrow$
181 0 we obtain $\omega_{ZQC} = 2\pi|J_{12}|$ and complete exchange is possible when $t = 1/(2J_{12})$.



182
183 **Figure 3.** Polarization transfer among two strongly coupled nuclei (A) in the absence and (B) in the presence (bottom)
184 of a heteronucleus. Here, we present the time dependence of $\langle I_{1z} \rangle$ (black solid lines) and $\langle I_{2z} \rangle$ (red dashed lines),
185 normalized to the initial value of $\langle I_{1z} \rangle$. The density operator at time $t = 0$ is $\sigma_0 = \hat{I}_{1z}$. Parameters of the simulation
186 were $\Delta\omega/2\pi = 10$ Hz, $J_{12} = 30$ Hz, and (a) $\Delta J = 0$ Hz and (b) $\Delta J = 100$ Hz.

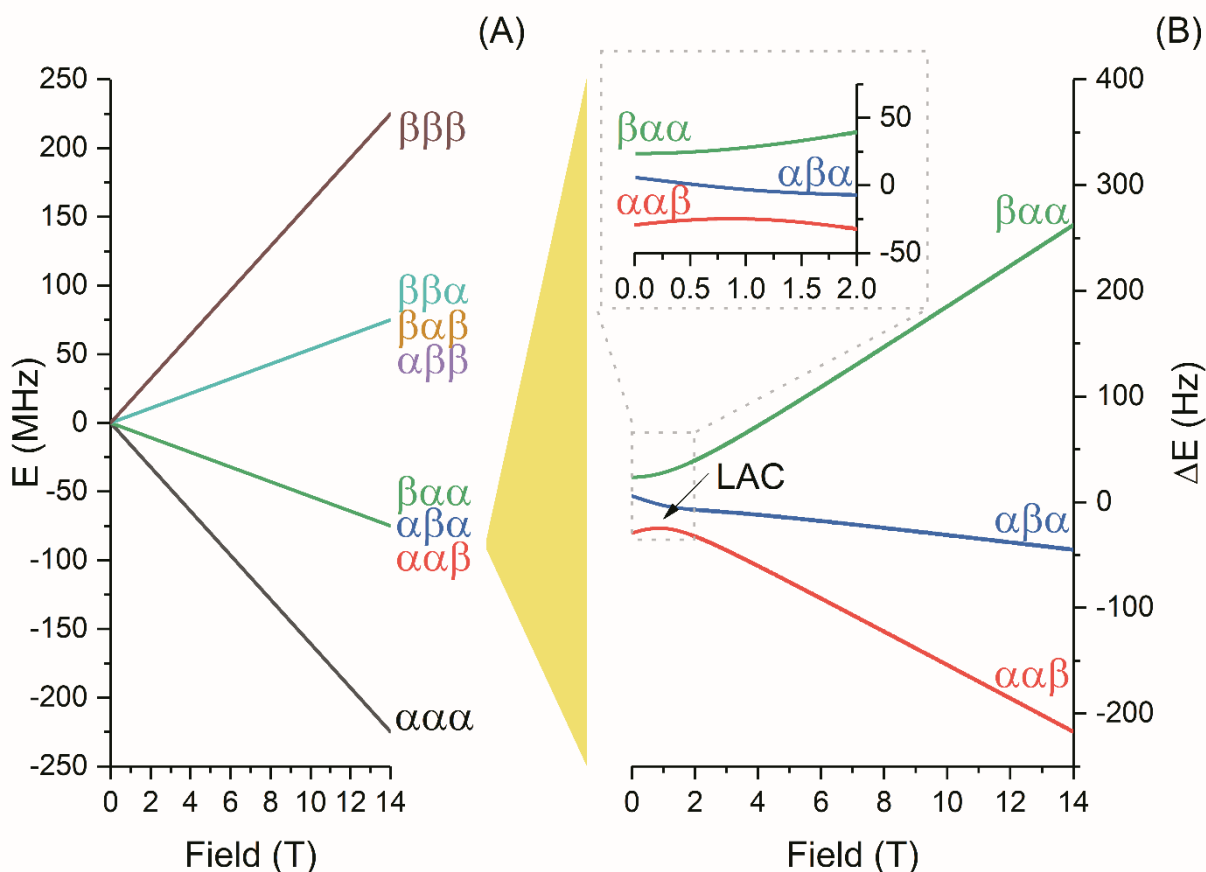
187 In the presence of scalar couplings to the third spin S , here a proton (I_1 and I_2 are carbon-13 nuclei), the
188 expressions should be modified: the evolution should be calculated for each specific spin state of the
189 proton, $|\alpha\rangle$ and $|\beta\rangle$, and sum of the two curves should be taken. We obtain at the following expression:

$$\begin{aligned} \langle I_{1z} \rangle(t) &= 1 - \sin^2 \theta_+ \frac{1 - \cos[\omega_{ZQC}^+ t]}{4} - \sin^2 \theta_- \frac{1 - \cos[\omega_{ZQC}^- t]}{4} \\ \langle I_{2z} \rangle(t) &= \sin^2 \theta_+ \frac{1 - \cos[\omega_{ZQC}^+ t]}{4} + \sin^2 \theta_- \frac{1 - \cos[\omega_{ZQC}^- t]}{4} \end{aligned} \quad (7)$$

190 where the evolution frequencies are equal to $\omega_{ZQC}^\pm = \sqrt{\Delta\omega_\pm^2 + (2\pi J_{12})^2}$.

191 The time dependence of the expectation value for the longitudinal polarizations of spins I_1 and I_2 is
192 presented in **Figure 3** in the presence and the absence of scalar couplings to a heteronucleus. In the
193 absence of heteronuclear coupling the two strongly coupled spins (the strong coupling condition is
194 fulfilled since $2\pi J_{12} > \Delta\omega$) almost completely exchange polarizations. The polarization transfer is of a

195 coherent nature and the frequency of the oscillations is given by the scalar-coupling constant J_{12} . In the
 196 presence of different heteronuclear scalar couplings to the third spin S , the time-evolution changes
 197 considerably. The two spins are no longer in the regime of strong coupling, since $|\Delta\omega_{\pm}| > 2\pi J_{12}$. The
 198 efficiency of polarization transfer is reduced and complete exchange of polarization is no longer possible.
 199 The time dependence also becomes more complex: instead of a single frequency ω_{ZQC} found in the
 200 previous case, here two frequencies appear: ω_{ZQC}^+ and ω_{ZQC}^- . Hence, when couplings to heteronuclei are
 201 present, the condition $\Delta\omega \sim 2\pi J_{12}$ does not guarantee that the homonuclei are in the strong-coupling
 202 regime.



203
 204 **Figure 4.** (A) Energy levels of the $\{C^{\gamma}, C^{\delta 1}, C^{\delta 2}\}$ spin system at variable magnetic field strength in the absence of
 205 scalar coupling with protons. Levels are assigned at high field, where the spin system is weakly coupled. (B) energy
 206 levels, corresponding to the $\alpha\alpha\beta$ and $\alpha\beta\alpha$ states at high field, have a LAC at 1.1 T, which is responsible for generation
 207 of the zero quantum coherences. To visualize the energy levels better, in the right panels we have subtracted the
 208 large Zeeman energy from the actual energy and show the energy difference. The calculation is done using
 209 parameters listed in [Table 1](#) and neglecting carbon-proton couplings.

210 These results show that the interaction with a heteronucleus clearly alters polarization transfer in strongly
 211 coupled networks. Consequently, we expect strong effects of heteronuclear interactions on polarization
 212 transfers in systems with several heteronuclei. Notably, we anticipate that polarization transfer among
 213 strongly coupled carbon spins will be dramatically different in the presence of proton decoupling, which
 214 effectively removes proton-carbon spin-spin interactions.

215 B. Spin dynamics simulations

216 In addition to this simple model, we carried out numerical simulations in a realistic multi-spin system: the
 217 isopropyl group of carbon-13 labeled leucine. This spin system contains three carbon-13 nuclei I_1, I_2 , and
 218 I_3 : the C^{γ} carbon-13 and the two C^{δ} carbon-13 nuclei. In addition, the spin system includes seven protons

219 S_i : each C^δ nucleus is coupled to the three protons of the methyl group, and the C^γ carbon-13 nucleus is
 220 coupled to one proton. We model the effects of fast field variation and coherent spin dynamics at low
 221 field. We consider two cases, namely, polarization transfer in the presence and in the absence of proton
 222 decoupling.

223 The simulation method is as follows. The band-selective inversion pulse on spin I_3 generates the initial
 224 density operator for the three-spin I system:

$$\sigma_0 = \sigma(t = 0) = \hat{I}_{1z} + \hat{I}_{2z} - \hat{I}_{3z} \quad (8)$$

225 Hence, we generate a population difference for the states $|\alpha\alpha\beta\rangle$, $|\alpha\beta\alpha\rangle$ and $|\beta\alpha\alpha\rangle$: the first state is
 226 overpopulated, while the other two states are underpopulated. The three-spin system under study, C^γ ,
 227 $C^{\delta 1}$ and $C^{\delta 2}$, has a LAC at $B = B_{LAC} \approx 1.1$ T, see [Figure 4](#). Upon passage through a LAC during the field
 228 jump $B_{HF} \rightarrow B_{LF}$ due to the sample shuttle transfer, the population difference is expected to be
 229 converted into a coherence between the states, which have the LAC: these adiabatic states correspond
 230 to the $|\alpha\alpha\beta\rangle$ and $|\alpha\beta\alpha\rangle$ states at high fields. To calculate the actual spin state at $B = B_{LF}$ we solve
 231 numerically the Liouville-von Neumann equation for the spin density operator

$$\frac{d}{dt}\sigma = -i[\hat{\mathcal{H}}(t), \sigma] \quad (9)$$

232 The Hamiltonian of the spin system at a magnetic field B is as follows:

$$\begin{aligned} \hat{\mathcal{H}}(B) = & -\gamma_C B \sum_{i=1}^3 (1 + \delta_{Ci}) \hat{I}_{iz} - \gamma_H B \sum_{j=1}^7 (1 + \delta_{Hj}) \hat{S}_{jz} + 2\pi \sum_{i \neq k} J_{Cik} (\hat{\mathbf{I}}_i \cdot \hat{\mathbf{I}}_k) \\ & + 2\pi \sum_{j \neq m} J_{Hjm} (\hat{\mathbf{S}}_j \cdot \hat{\mathbf{S}}_m) + 2\pi \sum_{i=1}^3 \sum_{j=1}^7 J'_{ij} \hat{I}_{iz} \hat{S}_{jz} \end{aligned} \quad (10)$$

233 Here γ_C and γ_H are the carbon and proton gyromagnetic ratios, δ_{Ci} and δ_{Hj} are the chemical shifts of the
 234 i -th carbon and j -th proton, J_{Cik} is the scalar coupling constant between the i -th and k -th carbon, J_{Hjm} is
 235 the scalar coupling constant between the j -th and m -th proton, J'_{ij} is the scalar coupling constant between
 236 the i -th carbon and j -th proton, $\hat{\mathbf{I}}_i$ and $\hat{\mathbf{S}}_j$ are the spin operator of the i -th carbon and j -th proton. Given
 237 the range of magnetic fields considered here, heteronuclear scalar couplings are considered to be weak.

238 **Table 1.** Parameters used for energy calculations. Proton-carbon direct scalar coupling values marked by asterisk
 239 have been used in numerical simulations of polarization transfer:

Chemical shifts	
C^γ	24.14 ppm
$C^{\delta 1}$	22.05 ppm
$C^{\delta 2}$	20.92 ppm
Scalar couplings	
$J(C^\gamma - C^{\delta 1})$	35 Hz
$J(C^\gamma - C^{\delta 2})$	35.4 Hz
$J(C^{\delta 1} - C^{\delta 2})$	0 Hz
$J(C^\gamma - H^\gamma)^*$	127.4 Hz
$J(C^{\delta 1} - H^{\delta 1})^*$	124.8 Hz
$J(C^{\delta 2} - H^{\delta 2})^*$	124.8 Hz

240 The precise values of the calculation parameters are given in [Table 1](#). Since the magnetic field B changes
 241 with time, the Hamiltonian $\hat{\mathcal{H}}$ is also time-dependent. In the calculation we consider three carbons and
 242 seven protons (six protons in three CH_3 -groups and the γ -proton). Using this Hamiltonian we evaluate the
 243 density operator after the first field jump, $\sigma(t = t_1)$. The Liouville-von Neumann equation is integrated

244 using 1 ms time increments and assuming that for each step the Hamiltonian is constant, similarly to
 245 simulations carried out for relaxation experiments (Bolik-Coulon et al., 2020). In the calculation, we ignore
 246 relaxation effects, since the dimensionality of the relaxation superoperator is too big for the multi-spin
 247 system considered here and our focus is on coherent effects.

248 At $B = B_{LF}$ the density operator evolves under a constant Hamiltonian, at the end of the evolution period
 249 it becomes as follows:

$$\sigma(t_1 + \tau) = \exp(-i\hat{\mathcal{H}}(B_{LF})\tau) \sigma(t_1) \exp(i\hat{\mathcal{H}}(B_{LF})\tau) \quad (11)$$

250 The $B_{LF} \rightarrow B_{HF}$ field jump is simulated numerically in the same way as the first field jump (the time
 251 interval is split into many small steps). Finally, knowing the density operator σ_{fin} at $t = t_1 + \tau + t_2$, we
 252 evaluate the NMR signals of the nuclei of interest as the expectation values of their z -magnetization
 253 $\langle I_{iz} \rangle = \text{Tr}\{\hat{I}_{iz}\sigma_{fin}\}$.

254 The method used for modelling the experiments with decoupling at $B = B_{LF}$ is different. After evaluating
 255 the density operator $\sigma(t = t_1)$ we trace out the proton degree of freedom and define the density
 256 operator of the carbon subsystem as $\sigma_C(t_1) = \text{Tr}_H\{\sigma(t_1)\}$, with the argument that proton polarization is
 257 destroyed by decoupling. The partial trace procedure implies that when $\sigma_{ik,jl}$ is a proton-carbon density
 258 operator (in the notation of spin states i, j stand for the proton states and k, l stand for the carbon states),
 259 the elements of the carbon density operator are: $\{\sigma_C\}_{k,l} = \sum_i \sigma_{ik,il}$. One should note that proton two-
 260 spin operators may contain a zero-quantum component, which would stand proton decoupling.
 261 Consideration of effects of such coherences is beyond the scope of this work: we expect this to only lead
 262 to small perturbations of the observed behavior. Then we introduce the Hamiltonian of the carbon
 263 subsystem

$$\hat{\mathcal{H}}_C(B_{LF}) = -\gamma_C B_{LF} \sum_{i=1}^3 (1 + \delta_{Ci}) \hat{I}_{iz} + 2\pi \sum_{i \neq k} J_{Cik} (\hat{\mathbf{I}}_i \cdot \hat{\mathbf{I}}_k) \quad (12)$$

264 Using this Hamiltonian, we evaluate the density operator of the ^{13}C spins at the end of the evolution period
 265 as follows

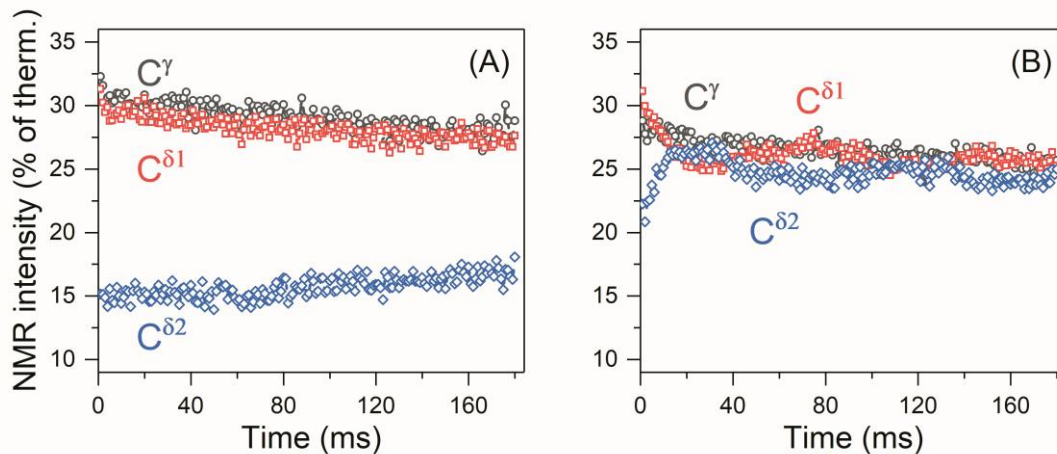
$$\sigma_C(t_1 + \tau) = \exp(-i\hat{\mathcal{H}}_C(B_{LF})\tau) \sigma_C(t_1) \exp(i\hat{\mathcal{H}}_C(B_{LF})\tau) \quad (13)$$

266 The final step in evaluating the ZQC evolution is introducing the carbon-proton density operator. This is
 267 done by multiplying $\sigma_C(t_1 + \tau)$ and the density operator of non-polarized protons (as decoupling removes
 268 any proton spin order). Hence,

$$\sigma(t_1 + \tau) = \sigma_C(t_1 + \tau) \otimes \sigma_H^{dec}, \quad \sigma_H^{dec} = \frac{1}{2^7} \prod_{j=1}^7 \hat{1} \quad (14)$$

269 where $\hat{1}$ is a 2×2 unity matrix. The final step of the calculation, the field jump $B_{LF} \rightarrow B_{HF}$, is modelled
 270 in the same way as in the previous case.

271 Finally, we would like to comment on the $B(t)$ dependence, which was used in calculation. The distance
 272 dependence of the magnetic field $B(z)$ is precisely known but the precise $z(t)$ is not known. We modelled
 273 this dependence assuming that motion goes with a constant speed (in experiments, constant-speed
 274 motion is achieved after a 5-10 ms lag delay for acceleration). Non-ideal agreement between theory and
 275 experiment can be attributed to the fact that the precise $z(t)$ dependence is not known (our previous
 276 works (Pravdivtsev et al., 2013; Kiryutin et al., 2013) show that the knowledge of $z(t)$ is required for
 277 modeling).



278
 279 **Figure 5.** Observed τ -dependence of the polarizations of carbon-13 nuclei C^γ , $C^{\delta 1}$ and $C^{\delta 2}$ measured (A) without ^1H
 280 decoupling, and (B) with ^1H decoupling. The NMR intensities are plotted in percent of the intensities of the NMR
 281 signals in the 150.9 MHz ^{13}C spectra (i.e., at 14.1 T) at thermal equilibrium.

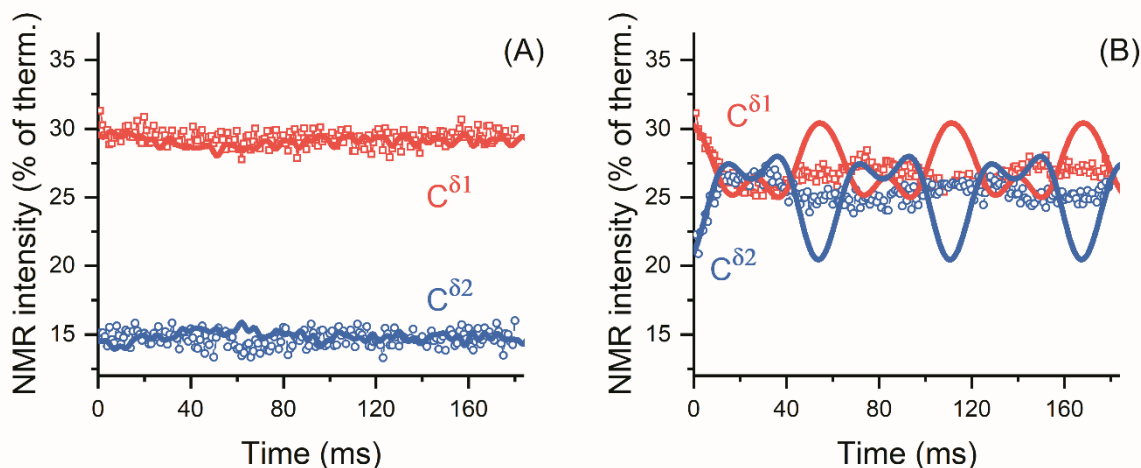
282 IV. Results and discussion

283 The experimental τ -dependences of the measured spin polarization are shown in **Figure 5**. One can see
 284 that without decoupling no coherent behavior is found: polarization simply decays due to relaxation and
 285 no coherent oscillations are visible (**Figure 5A**). In the presence of proton decoupling (**Figure 5B**) the
 286 situation is drastically different: coherent oscillations are clearly observed, which mediate polarization
 287 exchange between the $C^{\delta 1}$ and $C^{\delta 2}$ nuclei. We attribute such polarization exchange to the ZQC, which is
 288 generated by passage through the LAC. The coherence gives rise to exchange of the populations of the
 289 two states, which experience the LAC. These levels are correlated with the $|\alpha\alpha\beta\rangle$ and $|\alpha\beta\alpha\rangle$ high-field
 290 states. Hence, polarization transfer gives rise to population exchange of the states $|\alpha\alpha\beta\rangle$ (initially
 291 overpopulated state) and $|\alpha\beta\alpha\rangle$ (initially underpopulated state). As a result, the state of the first spin, C^γ ,
 292 does not change, but the other two spins, $C^{\delta 1}$ and $C^{\delta 2}$, exchange polarizations. With the available speed
 293 and range of the field-cycling, other coherences are not excited, i.e., non-adiabatic variation of the
 294 Hamiltonian is achieved only for the pairs of levels that have the LAC in between B_{LF} and B_{HF} , i.e., only
 295 the LAC shown in **Figure 4** contributes to spin mixing. The C^γ spin never shows any oscillatory polarization
 296 transfer, which is an indication that the specific LAC is responsible for the observed effect. In conclusion,
 297 a zero-quantum coherence of the two carbon-13 nuclei $C^{\delta 1}$ and $C^{\delta 2}$ is excited by fast magnetic field jump
 298 between 14.1 T and 0.33 T.

299 Hence, the oscillatory behavior does not show up in the absence of proton decoupling. There are two
 300 reasons for that. First, the multiple proton-carbon couplings give rise to a set of ZQC frequencies, instead
 301 of a unique frequency in the presence of decoupling. Second and more importantly, proton-carbon-13
 302 couplings prevent the carbon subsystem from reaching the strong-coupling regime. Thus, the amplitude
 303 of coherent evolutions is drastically reduced (see Eq. 7) and becomes negligible (**Figure 5A**). As a result,
 304 in experiments without decoupling the ZQC decays because of inhomogeneous broadening of the ZQC
 305 evolution frequency, *i.e.* relaxation. We would like to stress that the ZQC of interest is excited by the field
 306 jump, which is identical for experiments with and without proton decoupling at low field. However, the
 307 ZQC does not reveal itself and does not give rise to efficient polarization transfer in the experiment
 308 without decoupling.

309 These considerations are confirmed by theoretical modeling (**Figure 6**). In the presence of carbon-proton
 310 couplings coherent oscillations are hardly observed: only fast oscillations of very small amplitude can be
 311 seen in the simulated curves. By contrast, in the absence of the proton-carbon couplings, *i.e.*, when
 312 decoupling is used, coherent evolutions become manifest with slower oscillations of larger amplitude. The
 313 results of numerical modeling are in good agreement with the experimental data. As relaxation effects

314 are not taken into account in simulations, to ease comparison we subtracted the slowly relaxing
 315 background from the experimental time traces. In addition, we rescaled all calculated traces with the
 316 same factor; then the starting polarization values were adjusted individually to achieve the best
 317 agreement with the experimental data. Such a data treatment becomes necessary because relaxation is
 318 active not only during spin mixing at the B_{LF} field, but also during the field jumps. The agreement between
 319 the experimental data and simulation in **Figure 6** is not ideal, possibly because some small long-range
 320 scalar couplings are not included in the simulation but most likely because the field switching profile is
 321 not known exactly: previous studies of the spin dynamics in field-cycling NMR experiments (Pravdivtsev
 322 et al., 2013; Kiryutin et al., 2013) suggest that using the precise $B(t)$ profile is crucial for simulating
 323 coherent polarization transfer phenomena.



324 **Figure 6.** Calculated τ -dependence of polarization (lines) overlaid with the observed time traces (points) obtained
 325 (A) without ^1H decoupling, and (B) with ^1H decoupling. The slowly relaxing background (compare with the data shown
 326 in **Figure 5**) has been subtracted from the time traces, to enable comparison between theory and simulations. Observed NMR intensities are normalized to intensities in 150.9 MHz (14.1 T) ^{13}C spectra at thermal equilibrium. We
 327 use the subtraction procedure because relaxation effects were not taken into account in the calculation; consequently, we are unable to consider polarization decay due to relaxation at B_{LF} and during the field variation.
 328 To enable comparison of the experiment and calculation results, the amplitude of oscillations in polarization transfer
 329 traces were scaled with the same factor, then the starting polarization values were adjusted individually to give best
 330 agreement with experimental data.
 331
 332
 333

334 The absence of strong-coupling regime, in spite of scalar coupling constants larger than the difference in
 335 Larmor frequencies is somewhat counterintuitive but clearly explained when taking into account the
 336 effect of large heteronuclear scalar couplings (Eqs. 2-4). In the present case, the effect is even more
 337 pronounced, since the two δ carbon-13 nuclei of leucine are coupled to no less than 3 protons each,
 338 further splitting resonance frequencies in the absence of proton decoupling. A conventional way to
 339 present the weak coupling regime consists in stating that the part of the scalar coupling Hamiltonian (Eq.
 340 1) that is proportional to a zero-quantum product operator is non-secular in the frame of the Zeeman
 341 interactions of the two coupled spins, which is true if the scalar coupling constant is much smaller than
 342 the difference in Larmor frequencies of the two spins. Here, the weak-coupling regime is extended
 343 because this zero-quantum part can be considered non-secular in the interaction frame of the
 344 heteronuclear scalar couplings (note that the perturbative treatment is allowed to the extent that the
 345 heteronuclear coupling constants are much larger than the homonuclear coupling).

346 A particular consequence of the observation we report here can be relevant for experiments where the
 347 strong scalar-coupling regime is created by radio-frequency irradiation: isotropic mixing for TOCSY
 348 (Braunschweiler and Ernst, 1983). We have recently introduced a two-field TOCSY experiment where
 349 isotropic mixing is carried out at 0.33 T and chemical shift evolutions occur at high field (Kadeřávek et al.,
 350 2017), which makes broadband carbon-13 TOCSY straightforward. This study included a control

351 experiment where no radio-frequency pulses were applied at low field (see Figure 3.b in reference
352 (Kadeřávek et al., 2017). Intuitively, one would have expected cross-peaks to be observed for carbon-13
353 nuclei in strongly-coupled networks at 0.33 T. Some cross peaks could indeed be observed within the
354 aliphatic carbon region of leucine and in the aromatic ring of phenylalanine. The current investigation
355 suggests that strong scalar couplings between carbon-13 nuclei are less prevalent than expected at 0.33
356 T. The observed cross-peaks were possibly due to cross-relaxation and not necessarily coherent evolution
357 under strong scalar couplings. Conventional TOCSY experiments might also be altered by the effect of
358 large heteronuclear scalar couplings. In this case, isotropic mixing sequences have been optimized on
359 isolated pairs of two coupled spins (Kadkhodaie et al., 1991), excluding the effects of scalar couplings to
360 heteronuclei or as heteronuclear decoupling sequences that happen to be efficient at isotropic mixing
361 (Rucker and Shaka, 1989; Shaka et al., 1988). Although isotropic mixing sequences decouple heteronuclear
362 scalar couplings, optimizing simultaneously for homo- and heteronuclear scalar coupling operators may
363 improve homonuclear coherence transfers. Such effects of couplings to heteronuclei are of relevance for
364 abundant nuclei (protons), whereas for other nuclei they become important when uniform spin labelling
365 is used.

366 **V. Conclusions**

367 In this work, we present a study of coherent polarization transfer in a system of (strongly) coupled ^{13}C
368 nuclei. Spin coherences are zero-quantum coherences, which are generated by a fast non-adiabatic
369 magnetic field jump. Such coherences are excited most efficiently when the system goes through a LAC
370 during the field switch. Here we indeed pass through a LAC in a system of three coupled ^{13}C spins and
371 investigate the spin dynamics at low fields, where strong couplings of the carbon spins are expected.

372 We can clearly demonstrate that the polarization transfer in the carbon-13 spin subsystem is strongly
373 affected by spin-spin interactions with the protons in the molecule. In this situation, the role of these
374 interactions can be determined by comparing the experiments with and without proton decoupling at low
375 fields. When decoupling is used, we observe coherent polarization exchange between two of the three
376 carbons: such a behavior is typical when the spin coherences are excited upon non-adiabatic passage
377 through a specific LAC. In the absence of decoupling, i.e., when heteronuclear interactions are present,
378 we cannot observe such a behavior: polarization transfer is very inefficient and coherent phenomena are
379 not found. We attribute this to the fact that relatively strong proton-carbon couplings (i) drive the carbon
380 system away from the strong coupling condition and (ii) give rise to a set of evolution frequencies instead
381 of a unique ZQC frequency. These considerations are supported by an analytical model of a three-spin
382 system and numerical simulations in a multi-spin system.

383 Our results are of importance for analyzing polarization transfer phenomena at low magnetic fields and
384 for interpreting NMR data obtained under apparent strong coupling conditions. Under such conditions
385 heteronuclear spin-spin interactions might disturb “strong coupling” of homonuclei and substantially alter
386 spin dynamics. Similar effects also often arise in dynamic nuclear polarization, where the difference in the
387 electron-nuclear couplings for nuclei located at different distances from the electron hampers nuclear
388 spin diffusion, giving rise to the spin diffusion barrier around the electron spin (Ramanathan, 2008).

389 **Acknowledgements**

390 This work has been supported by the Russian Foundation for Basic Research (grants Nos. 19-29-10028 and
391 19-33-90251). I.V.Z. acknowledges support from the French embassy in the Russian Federation, in the
392 framework of the Ostrogradsky fellowship (project No. 933824A).

393 **References**

394 Appelt, S., Häsing, F. W., Sieling, U., Gordji-Nejad, A., Glöggler, S., and Blümich, B.: Paths from Weak to
395 Strong Coupling in NMR, *Phys. Rev. A*, 81, 023420, <https://doi.org/10.1103/PhysRevA.81.023420>, 2010.

396 Blanchard, J. W., and Budker, D.: Zero- to Ultralow-Field NMR, *eMagRes*, 5, 1395-1409,
397 <https://doi.org/10.1002/9780470034590.emrstm1369>, 2016.

398 Bodenhausen, G., Freeman, R., Morris, G. A., and Turner, D. L.: Proton-Coupled Carbon-13 J Spectra in the
399 Presence of Strong Coupling. II, *J. Magn. Reson.*, 28, 17-28, [https://doi.org/10.1016/0022-2364\(77\)90252-](https://doi.org/10.1016/0022-2364(77)90252-9)
400 9, 1977.

401 Bolik-Coulon, N., Kaderavek, P., Pelupessy, P., Dumez, J. N., Ferrage, F., and Cousin, S. F.: Theoretical and
402 Computational Framework for the Analysis of the Relaxation Properties of Arbitrary Spin Systems.
403 Application to High-Resolution Relaxometry, *J. Magn. Reson.*, 313,
404 <https://doi.org/10.1016/j.jmr.2020.106718>, 2020.

405 Braunschweiler, L., and Ernst, R. R.: Coherence Transfer by Isotropic Mixing - Application to Proton
406 Correlation Spectroscopy, *J. Magn. Reson.*, 53, 521-528, [https://doi.org/10.1016/0022-2364\(83\)90226-3](https://doi.org/10.1016/0022-2364(83)90226-3),
407 1983.

408 Bryant, R. G., and Korb, J. P.: Nuclear Magnetic Resonance and Spin Relaxation in Biological Systems,
409 *Magn. Reson. Imaging*, 23, 167-173, <https://doi.org/10.1016/j.mri.2004.11.026>, 2005.

410 Cavanagh, J.: *Protein NMR Spectroscopy : Principles and Practice*, 2nd ed., Academic Press, Amsterdam ;
411 Boston, xxv, 885 p. pp., 2007.

412 Charlier, C., Khan, S. N., Marquardsen, T., Pelupessy, P., Reiss, V., Sakellariou, D., Bodenhausen, G.,
413 Engelke, F., and Ferrage, F.: Nanosecond Time Scale Motions in Proteins Revealed by High-Resolution NMR
414 Relaxometry, *J. Am. Chem. Soc.*, 135, 18665-18672, <https://doi.org/10.1021/ja409820g>, 2013.

415 Chou, C.-Y., Chu, M., Chang, C.-F., Yu, T., Huang, T.-h., and Sakellariou, D.: High Sensitivity High-Resolution
416 Full Range Relaxometry Using a Fast Mechanical Sample Shuttling Device and a Cryo-Probe, *J. Biomol.*
417 *NMR*, 66, 187-194, <https://doi.org/10.1007/s10858-016-0066-5>, 2016.

418 Chou, C.-Y., Abdesselem, M., Bouzigues, C., Chu, M., Guiga, A., Huang, T.-H., Ferrage, F., Gacoin, T.,
419 Alexandrou, A., and Sakellariou, D.: Ultra-Wide Range Field-Dependent Measurements of the Relaxivity
420 of Gd_{1-x}Eu_xVO₄ Nanoparticle Contrast Agents Using a Mechanical Sample-Shuttling Relaxometer, *Sci. Rep.*,
421 7, 44770, <https://doi.org/10.1038/srep44770>, 2017.

422 Cousin, S. F., Charlier, C., Kaderavek, P., Marquardsen, T., Tyburn, J. M., Bovier, P. A., Ulzega, S., Speck, T.,
423 Wilhelm, D., Engelke, F., Maas, W., Sakellariou, D., Bodenhausen, G., Pelupessy, P., and Ferrage, F.: High-
424 Resolution Two-Field Nuclear Magnetic Resonance Spectroscopy, *Phys. Chem. Chem. Phys.*, 18, 33187-
425 33194, <https://doi.org/10.1039/c6cp05422f>, 2016a.

426 Cousin, S. F., Kaderavek, P., Haddou, B., Charlier, C., Marquardsen, T., Tyburn, J. M., Bovier, P. A., Engelke,
427 F., Maas, W., Bodenhausen, G., Pelupessy, P., and Ferrage, F.: Recovering Invisible Signals by Two-Field
428 NMR Spectroscopy, *Angew. Chem., Int. Ed.*, 55, 9886-9889, <https://doi.org/10.1002/anie.201602978>,
429 2016b.

430 Ernst, R. R., Bodenhausen, G., and Wokaun, A.: *Principles of Nuclear Magnetic Resonance in One and Two*
431 *Dimensions*, The International Series of Monographs on Chemistry, 14, Clarendon Press; Oxford University
432 Press, Oxford Oxfordshire, New York, 1987.

433 Foroozandeh, M., Adams, R. W., Meharry, N. J., Jeannerat, D., Nilsson, M., and Morris, G. A.: Ultrahigh-
434 Resolution NMR Spectroscopy, *Angew. Chem., Int. Ed.*, 53, 6990-6992,
435 <https://doi.org/10.1002/anie.201404111>, 2014.

436 Geen, H., and Freeman, R.: Band-Selective Radiofrequency Pulses, *J. Magn. Reson.*, 93, 93-141,
437 [https://doi.org/10.1016/0022-2364\(91\)90034-Q](https://doi.org/10.1016/0022-2364(91)90034-Q), 1991.

438 Goddard, Y., Korb, J.-P., and Bryant, R. G.: The Magnetic Field and Temperature Dependences of Proton
439 Spin-Lattice Relaxation in Proteins, *J. Chem. Phys.*, 126, 175105, <https://doi.org/10.1063/1.2727464>,
440 2007.

441 Grootveld, M., Percival, B., Gibson, M., Osman, Y., Edgar, M., Molinari, M., Mather, M. L., Casanova, F.,
442 and Wilson, P. B.: Progress in Low-Field Benchtop NMR Spectroscopy in Chemical and Biochemical
443 Analysis, *Anal. Chim. Acta*, 1067, 11-30, <https://doi.org/10.1016/j.aca.2019.02.026>, 2019.

444 Ivanov, K. L., Miesel, K., Yurkovskaya, A. V., Korchak, S. E., Kiryutin, A. S., and Vieth, H.-M.: Transfer of
445 CIDNP among Coupled Spins at Low Magnetic Field, *Appl. Magn. Reson.*, 30, 513-534,
446 <https://doi.org/10.1007/Bf03166215>, 2006.

447 Ivanov, K. L., Yurkovskaya, A. V., and Vieth, H.-M.: Coherent Transfer of Hyperpolarization in Coupled Spin
448 Systems at Variable Magnetic Field, *J. Chem. Phys.*, 128, 154701, <https://doi.org/10.1063/1.2901019>,
449 2008.

450 Ivanov, K. L., Pravdivtsev, A. N., Yurkovskaya, A. V., Vieth, H.-M., and Kaptein, R.: The Role of Level Anti-
451 Crossings in Nuclear Spin Hyperpolarization, *Prog. Nucl. Magn. Reson. Spectrosc.*, 81, 1-36,
452 <https://doi.org/10.1016/j.pnmrs.2014.06.001>, 2014.

453 Kadeřávek, P., Strouk, L., Cousin, S. F., Charlier, C., Bodenhausen, G., Marquardsen, T., Tyburn, J. M.,
454 Bovier, P. A., Engelke, F., Maas, W., and Ferrage, F.: Full Correlations across Broad NMR Spectra by Two-
455 Field Total Correlation Spectroscopy, *ChemPhysChem*, 18, 2772-2776,
456 <https://doi.org/10.1002/cphc.201700369>, 2017.

457 Kadkhodaie, M., Rivas, O., Tan, M., Mohebbi, A., and Shaka, A. J.: Broad-Band Homonuclear Cross
458 Polarization Using Flip-Flop Spectroscopy, *J. Magn. Reson.*, 91, 437-443, [https://doi.org/10.1016/0022-2364\(91\)90210-K](https://doi.org/10.1016/0022-2364(91)90210-K), 1991.

460 Keeler, J.: *Understanding NMR Spectroscopy*, Wiley, Chichester, England; Hoboken, NJ, xv, 459 p. pp.,
461 2005.

462 Kiryutin, A. S., Yurkovskaya, A. V., Kaptein, R., Vieth, H.-M., and Ivanov, K. L.: Evidence for Coherent
463 Transfer of Para-Hydrogen-Induced Polarization at Low Magnetic Fields, *J. Phys. Chem. Lett.*, 4, 2514-
464 2519, <https://doi.org/10.1021/jz401210m>, 2013.

465 Kiryutin, A. S., Pravdivtsev, A. N., Ivanov, K. L., Grishin, Y. A., Vieth, H.-M., and Yurkovskaya, A. V.: A Fast
466 Field-Cycling Device for High-Resolution NMR: Design and Application to Spin Relaxation and
467 Hyperpolarization Experiments, *J. Magn. Reson.*, 263, 79-91, <https://doi.org/10.1016/j.jmr.2015.11.017>,
468 2016.

469 Korchak, S. E., Ivanov, K. L., Pravdivtsev, A. N., Yurkovskaya, A. V., Kaptein, R., and Vieth, H.-M.: High
470 Resolution NMR Study of T_1 Magnetic Relaxation Dispersion. III. Influence of Spin 1/2 Hetero-Nuclei on
471 Spin Relaxation and Polarization Transfer among Strongly Coupled Protons, *J. Chem. Phys.*, 137, 094503,
472 <https://doi.org/10.1063/1.4746780>, 2012.

473 Ledbetter, M. P., Theis, T., Blanchard, J. W., Ring, H., Ganssle, P., Appelt, S., Blümich, B., Pines, A., and
474 Budker, D.: Near-Zero-Field Nuclear Magnetic Resonance, *Phys. Rev. Lett.*, 107, 107601,
475 <https://doi.org/10.1103/PhysRevLett.107.107601>, 2011.

476 Levitt, M. H., Freeman, R., and Frenkiel, T.: Supercycles for Broad-Band Heteronuclear Decoupling, *J.*
477 *Magn. Reson.*, 50, 157-160, [https://doi.org/10.1016/0022-2364\(82\)90042-7](https://doi.org/10.1016/0022-2364(82)90042-7), 1982.

478 Levitt, M. H.: *Spin Dynamics : Basics of Nuclear Magnetic Resonance-2nd Ed.*, 2008.

479 Miesel, K., Ivanov, K. L., Yurkovskaya, A. V., and Vieth, H.-M.: Coherence Transfer During Field-Cycling NMR
480 Experiments, *Chem. Phys. Lett.*, 425, 71-76, <https://doi.org/10.1016/j.cplett.2006.05.025>, 2006.

481 Pfändler, P., and Bodenhausen, G.: Strong Coupling Effects in Z-Filtered Two-Dimensional NMR
482 Correlation Spectra, *J. Magn. Reson.*, 72, 475-492, [https://doi.org/10.1016/0022-2364\(87\)90152-1](https://doi.org/10.1016/0022-2364(87)90152-1), 1987.

483 Pravdivtsev, A. N., Yurkovskaya, A. V., Kaptein, R., Miesel, K., Vieth, H.-M., and Ivanov, K. L.: Exploiting
484 Level Anti-Crossings for Efficient and Selective Transfer of Hyperpolarization in Coupled Nuclear Spin
485 Systems, *Phys. Chem. Chem. Phys.*, 15, 14660-14669, <https://doi.org/10.1039/c3cp52026a>, 2013.

486 Ramanathan, C.: Dynamic Nuclear Polarization and Spin Diffusion in Nonconducting Solids, *Appl. Magn.*
487 *Reson.*, 34, 409-421, 2008.

488 Redfield, A. G.: High-Resolution NMR Field-Cycling Device for Full-Range Relaxation and Structural Studies
489 of Biopolymers on a Shared Commercial Instrument, *J. Biomol. NMR*, 52, 159-177,
490 <https://doi.org/10.1007/s10858-011-9594-1>, 2012.

491 Roberts, M. F., and Redfield, A. G.: Phospholipid Bilayer Surface Configuration Probed Quantitatively by
492 ^{31}P Field-Cycling NMR, *Proc. Natl. Acad. Sci. U. S. A.*, 101, 17066-17071, <https://doi.org/10.1007/s10858-011-9594-1>, 2004a.

494 Roberts, M. F., and Redfield, A. G.: High-Resolution ^{31}P Field Cycling NMR as a Probe of Phospholipid
495 Dynamics, *J. Am. Chem. Soc.*, 126, 13765-13777, <https://doi.org/10.1021/ja046658k>, 2004b.

496 Rucker, S. P., and Shaka, A. J.: Broad-Band Homonuclear Cross Polarization in 2D NMR Using DIPSI-2, *Mol.*
497 *Phys.*, 68, 509-517, <https://doi.org/10.1080/00268978900102331>, 1989.

498 Shaka, A. J., Keeler, J., Frenkiel, T., and Freeman, R.: An Improved Sequence for Broad-Band Decoupling -
499 WALTZ-16, *J. Magn. Reson.*, 52, 335-338, [https://doi.org/10.1016/0022-2364\(83\)90207-X](https://doi.org/10.1016/0022-2364(83)90207-X), 1983.

500 Shaka, A. J., Lee, C. J., and Pines, A.: Iterative Schemes for Bilinear Operators - Application to Spin
501 Decoupling, *J. Magn. Reson.*, 77, 274-293, [https://doi.org/10.1016/0022-2364\(88\)90178-3](https://doi.org/10.1016/0022-2364(88)90178-3), 1988.

502 Tayler, M. C. D., Theis, T., Sjolander, T. F., Blanchard, J. W., Kentner, A., Pustelny, S., Pines, A., and Budker,
503 D.: Invited Review Article: Instrumentation for Nuclear Magnetic Resonance in Zero and Ultralow
504 Magnetic Field, *Rev. Sci. Instrum.*, 88, 091101, <https://doi.org/10.1063/1.5003347>, 2017.
505 Türschmann, P., Colell, J., Theis, T., Blümich, B., and Appelt, S.: Analysis of Parahydrogen Polarized Spin
506 System in Low Magnetic Fields, *Phys. Chem. Chem. Phys.*, 16, 15411-15421,
507 <https://doi.org/10.1039/c4cp01807a>, 2014.
508 Vallurupalli, P., Scott, L., Williamson, J. R., and Kay, L. E.: Strong Coupling Effects During X-Pulse CPMG
509 Experiments Recorded on Heteronuclear ABX Spin Systems: Artifacts and a Simple Solution, *J. Biomol.*
510 *NMR*, 38, 41-46, <https://doi.org/10.1007/s10858-006-9139-1>, 2007.
511 Wagner, S., Dinesen, T. R. J., Rayner, T., and Bryant, R. G.: High-Resolution Magnetic Relaxation Dispersion
512 Measurements of Solute Spin Probes Using a Dual-Magnet System, *J. Magn. Reson.*, 140, 172-178,
513 <https://doi.org/10.1006/jmre.1999.1811>, 1999.
514 Zhukov, I. V., Kiryutin, A. S., Yurkovskaya, A. V., Grishin, Y. A., Vieth, H.-M., and Ivanov, K. L.: Field-Cycling
515 NMR Experiments in Ultra-Wide Magnetic Field Range: Relaxation and Coherent Polarization Transfer,
516 *Phys. Chem. Chem. Phys.*, 20, 12396-12405, <https://doi.org/10.1039/C7CP08529J>, 2018.